RPE | Radiation Physics & Engineering
A Peer-Reviewed Journal
Published by K.N. Toosi University of Technology
http://rpe.kntu.ac.ir
Research Article

Radiation Physics and Engineering 2023; 4(1):29–38

Low-energy deuteron-deuteron elastic scattering in cluster effective field theory

Mohammadhosein Farzin[a], Mahdi Radin[a,*], Mahdi Moeini Arani[b]

[a] *Department of Physics, K.N. Toosi University of Technology, P.O. Box 16315-1618, Tehran, Iran*
[b] *Malek Ashtar University of Technology, Tehran, Iran*

HIGHLIGHTS

- The two-body cluster EFT is used to study the low-energy d-d elastic scattering up to NLO.
- The unknown EFT low-energy coupling constants are determined up o NLO.
- The obtained phase shifts and differential cross section results are compared to the experimental data.

ABSTRACT

We study the low-energy deuteron-deuteron elastic scattering using the cluster effective field theory formalism up to next-to-leading order (NLO). For this purpose, we initially focus on determination of the unknown effective field theory coupling constant values using the phase shift analysis and available differential cross section data. The differential cross section versus center of mass energy and scattering angle are plotted up to NLO in the suggested power counting and compared to the available experimental data. Our effective field theory results show good consistency with the experimental data.

KEYWORDS

Elastic scattering
Coulomb interaction
Cross section
Phase shift

HISTORY

Received: 21 November 2022
Revised: 14 December 2022
Accepted: 14 December 2022
Published: Winter 2023

1 Introduction

The main expedient of describing the interaction between the light nuclei such as d-d, d$-^3$He, d$-^3$H, d$-^4$He, ^{3}H$-^3$He, and others is the subject of some theoretical studies. Also, astrophysical radiative capture precesses, e.g. deuteron-deuteron (d-d) radiative capture reaction, are known as theoretically interesting reactions. In the present work, we focus on applying the effective field theory (EFT) formalism as a model independent, systematic and controlled-precision procedure to investigation of d-d elastic scattering at center of mass (c.m.) energies about a few MeV corresponding to the validity of EFT expansion and the consideration of deuterons as point-like nuclear clusters. The evaluated results can help us to investigate the astrophysical radiative capture processes d+d$\rightarrow^4$He+γ using halo/cluster in the future.

The applications of EFT approach in the few-nucleon systems have widely studied (Bedaque and Van Kolck, 2002; Braaten and Hammer, 2006; Kaplan et al., 1998; Phillips et al., 2000; Chen et al., 1999). Resently, the nuclear systems with $A > 4$ which can be classified in the two-body sector are extensively studied by halo EFT scheme (Hammer et al., 2017). The deuteron can be considered as a simplest halo nucleus which core is a nucleon, however, there are some EFT works that the deuteron field is introduced as an elementary-like field (Ando, 2014; Ando et al., 2014; Arani et al., 2017a; Arani, 2020). Halo EFT captures the physics of resonantly P-wave interactions in neutron-alpha scattering up to next-to-leading order (NLO) (Bertulani et al., 2002; Bedaque et al., 2003) and studying two-neutron halo system ^{6}He (Ji et al., 2014; Arani et al., 2017b). The effects of the Coulomb interaction in two-body systems such as proton-proton (p-p) (Kong and Ravndal, 1999, 2000; Barford and Birse, 2003; Ando et al., 2007; Ando and Birse, 2008), p-^{7}Li (Lensky and Birse, 2011), $\alpha-^{12}$C (Ando, 2016), and alpha-alpha ($\alpha-\alpha$) scattering (Higa et al., 2008) and ^{3}He$(\alpha,\gamma)^7$Be

*Corresponding author: radin@kntu.ac.ir

https://doi.org/10.22034/rpe.2022.371177.1109
https://dorl.net/dor/20.1001.1.26456397.2023.4.1.5.9

(Higa et al., 2018), have been considered by the EFT approach.

The phase shift analysis and differential cross section calculation for the d-d elastic scattering procedure, after determination of the unknown EFT low-energy coupling constants (LECs), are the main purposes of this paper. We obtain the EFT LECs by using available experimental data and theoretical results for d-d elastic scattering in the low energies. In the very low-energy region, $E_d = 80-360$ keV, measurement of the cross section have been done (Marlinghaus et al., 1975; Niewisch and Fick, 1975). These studies provided no evidence for a resonance near d-d threshold. Since the earlier compilation on the $A = 4$ system, a considerable amount of theoretical work on ^{2}H(d,d)^{2}H elastic scattering has been done (Meier and Glöckle, 1975). A resonating group method (RGM) with imaginary potential was applied to d-d scattering (Burke and Laskar, 1961; Thompson, 1970; Chwieroth et al., 1972; Xuan and Fan-An, 1985).

Our paper is organized as follows. In Sec. 2 we introduce the long-range Coulomb interaction and strong effective Lagrangian for the d-d system at low energies. The halo EFT calculation of leading order (LO) and NLO scattering amplitudes together with the pure-Coulomb scattering amplitude are presented in Sec. 3. Sec. 4 is allocated to determination of the values of unknown EFT coupling constants for all spin singlet, triplet and quintet partial wave channels using the available scattering data. In Sec. 5 the LO and NLO EFT results for the differential cross sections in terms of c.m. energy and scattering angle are indicated and compared with the available experimental data. We summarize the paper and discuss extension of the investigation to other few-body systems in Sec. 6.

2 Interaction

According to the spin of deuteron ($S = 1$), two deuterons can meet in 9 distinct spin states, classifiable into the singlet, triplet and quintet states. According to the isospin of deuteron ($T = 0$) and Considering the l-wave components of d-d system, the antisymmetrized wave function have $S = 0, 2$ with even l and $S = 1$ with odd l. At low energies, only S- and P-waves are important so, there are two S-waves ($^1S_0$, $^5S_2$) and three P-waves ($^3P_0$, $^3P_1$, and $^3P_2$ corresponding to total angular momentums $J = 0$, 1, and 2). At the present low-energy approach, we present the classification by orbital symmetries of the d-d system. So, we have generally 3 distinguishable channels $^1S_0$, $^5S_2$ and ^3P which contribute to the deuteron-deuteron scattering amplitude.

It is noted that the deuteron cluster is very weakly bound; hence, it can be easily decomposed in the strong interaction region of d-d interaction. The main difficulty in the d-d scattering problem arises from the loose binding of the deuteron cluster and thus any pair of deuterons in a strong interaction region distort each other very violently. This distortion inserts the contributions of the proton-^{3}H(p-t) and neutron-^{3}He(n-τ) interactions in the d-d elastic scattering amplitude specially by increasing the incoming energy. The cluster EFT that we construct treats the deuterons as the point-like nuclear clusters which can make dimerons in the S- and P-waves $^1S_0$, $^5S_2$ and ^3P. Therefore, the d-d system is investigated as two-body cluster and the effects of the n-τ and p-t channels will be omitted.

Taking into consideration two deuterons as two charged nuclear clusters, we have generally both long-range Coulomb force and short-range strong interaction for the d-d system. We describe these interactions in the following sections.

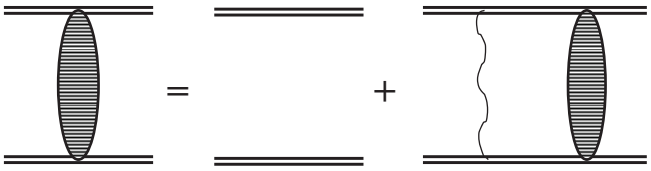

Figure 1: The Coulomb Green's function. The wavy and double lines depict a deuteron and a photon, respectively.

2.1 Coulomb force

For low-energy scattering of two charged deuterons, the strength of Coulomb photon exchange is provided by the Sommerfeld parameter $\eta_p = k_C/p$, where p is the relative momentum of two deuterons in c.m. frame and k_C is the inverse of the Bohr radius of the system which is given for d-d interaction as $k_C = \alpha_{em}\,\mu \sim 7$ MeV. $\alpha_{em} = e^2/4\pi \sim 1/137$ indicates the fine-structure constant and μ denotes the reduced mass of d-d system. Based on the fact that each photon-exchange insertion is proportional to η_p so, in the current low-energy scattering process, $p \sim k_C$, we should consider the full Coulomb interaction including all multiple photon exchange at the same order as depicted in Fig. 1. The free and Coulomb green's function for d-d system are respectively given by

$$\hat{G}_0^{\pm}(E) = \frac{1}{E - \hat{H}_0 \pm i\epsilon}$$
$$\hat{G}_C^{\pm}(E) = \frac{1}{E - \hat{H}_0 - \hat{V}_C \pm i\epsilon} \quad (1)$$

where $V_C = \alpha_{em}/r$ and $\hat{H}_0 = \hat{p}^2/2\mu$ are the repulsive Coulomb potential between two deuterons and the free Hamiltonian, respectively. The Coulomb green's function for two-deuteron can be related to the free green's function using the integral equation

$$\hat{G}_C^{\pm} = \hat{G}_0^{\pm} + \hat{G}_0^{\pm}\hat{V}_C\,\hat{G}_C^{\pm} \quad (2)$$

which shows an infinite sum of Feynman diagrams as indicated in Fig. 1. The incoming and outgoing Coulomb wave functions can be obtain by solving the Schrodinger equation with the full Hamiltonian $\hat{H} = \hat{H}_0 + \hat{V}_C$ as (Gasser et al., 2008; Goldberger and Watson, 2004; Weiss, 1958)

$$\psi_p^{(\pm)}(\vec{r}) = \mathrm{e}^{-\frac{1}{2}\pi\eta_p}\Gamma(1 \pm i\eta_p) \times M(\mp i\eta_p, 1, \pm ipr - i\vec{p}\cdot\vec{r})\,\mathrm{e}^{i\vec{p}\cdot\vec{r}} \quad (3)$$

where $M(a,b;x)$ is well-known as the Kummer function.

According to the Coulomb wave functions (Eq. (3)), the useful expressions in the next calculations for the non-perturbative Coulomb corrections of the strong scattering amplitude can be derived as

$$\begin{aligned}\psi_{p'}^{(\mp)*}(\vec{0})\,\psi_{p}^{(\pm)}(\vec{0}) &= C_0^2(\eta_p)\mathrm{e}^{\pm 2i\sigma_0}\\ \left[\vec{\nabla}\psi_{p'}^{(\mp)*}(\vec{0})\right]\cdot\left[\vec{\nabla}\psi_{p}^{(\pm)}(\vec{0})\right] &= C_0^2(\eta_p)(1+\eta_p^2)\,\vec{p}\cdot\vec{p}'\mathrm{e}^{\pm 2i\sigma_1}\\ \left[\vec{\nabla}\psi_{p}^{(\pm)*}(\vec{0})\right]\cdot\left[\vec{\nabla}\psi_{p}^{(\pm)}(\vec{0})\right] &= C_0^2(\eta_p)(p^2+k_C^2)\end{aligned} \tag{4}$$

where the Sommerfeld factor $C_0^2(\eta_p)$, the probability to find the two interacting particles at zero separation, is given by

$$C_0^2(\eta_p) = |\psi_p^{(\pm)}(\vec{0})|^2 = \frac{2\pi\eta_p}{\mathrm{e}^{2\pi\eta_p}-1} \tag{5}$$

and

$$\sigma_l = \arg\Gamma(l+1+i\eta_p) = \frac{1}{2i}\left[\frac{\Gamma(l+1+i\eta_p)}{\Gamma(l+1-i\eta_p)}\right] \tag{6}$$

is the Coulomb phase shift for l partial wave.

2.2 Strong interaction

Neglecting the relativistic corrections and the effects of the pion exchange, the degrees of freedom for the d-d scattering process in the current halo EFT study are the deuterons as a point-like nuclear cluster. In this low-energy formalism, the relative momentum of two deuterons, $p \le k_C$, scales as a low-momentum Q. Here, the breakdown momentum scale Λ is also set by the lowest-energy degrees of freedom that have been integrated out. With respect to no existing explicit pions and any deuteron deformations, Λ is the smallest between the pion mass $m_\pi \sim 140$ MeV and the c.m. momentum corresponding to the deuteron binding energy ($E_{cm}^d \sim -B_d = \Lambda^2/2m_d$). So, the high-momentum scale would be considered as $\Lambda \sim \sqrt{2m_d B_d} \sim 90$ MeV.

Around the $p \sim k_C \sim 7$ MeV, we expect an expansion parameter of the order of 1/12. By increasing the energy the expansion deteriorates and the precision of the EFT prediction will be questionable for $E_{cm} = p^2/2\mu > 4$ MeV. A reliable estimate regards to the momentums lower than 60 MeV. In the present study, we focus on the d-d scattering at low energies $0 < E_{cm} \le 2$ MeV corresponding to the momentums $0 < p \le 60$ MeV. The Sommerfeld parameter η_p is enhanced by decreasing the energy. So, η_p would be large around $p \lesssim k_C$ and the elastic scattering amplitude requires non-perturbative treatment of the Coulomb photons. Furthermore, the large value of η_p leads to $2k_C H(\eta_p) \sim p^2/6k_C$ (Higa et al., 2008). For the S-wave channels, $2k_C H(\eta_p)$ is comparable in magnitude to the effective-range term and can be automatically captured by taking $3k_C \sim \Lambda$. In the P-waves, we have $2k_C(p^2+k_C^2)H(\eta_p) \sim p^2 k_C/6 + p^4/6k_C$ and the term including $H(\eta_p)$ can be also managed by scaling $k_C/3 \sim Q$ and $2/3k_C \sim 1/\Lambda$.

Table 1: The suggested power-counting for effective range parameters. Q and Λ denote the low- and high-momentum scales as introduced in the text.

ξ	$1/a^{[\xi]}$	$r^{[\xi]}/2$	$s^{[\xi]}/4$
$^1S_0$	Λ	$1/\Lambda$	$1/\Lambda^2 Q$
$^5S_2$	Λ	$1/\Lambda$	$1/\Lambda^3$
^3P	Q^4/Λ	Q^4/Λ^3	$1/\Lambda$

As discussed, at low energies the Coulomb photons enter non-pertubatively. However, it is not clear if the short-range strong interaction in terms of effective range parameters should be included in perturbation or not. Fitting the EFT expression to the phase shifts and cross section data in the following section, we propose a power-counting (PC) that the effective-range parameters of ξ channel are scaled as presented in Table 1. The LO contribution of the scattering amplitude in each channel comes clearly from both its scattering length and effective range and its shape parameter influence is considered at NLO. According to the scaling the effective-range parameters of ξ channel as indicated in Table 1, the LO differential cross section of the d-d elastic scattering is dominantly constructed by the scattering length and effective range of $^5S_2$ channel. The $s^{[^5S_2]}$ and the remained effective range parameters enter as the higher-order corrections in total cross section.

The Lagrangian of the strong d-d interaction up to NLO is given by

$$\begin{aligned}\mathcal{L}^{[\xi]} = {} & d_i^\dagger\Big(i\partial_0 + \frac{\vec{\nabla}^2}{2m_d}\Big)d^i + \eta^{[\xi]}T^{[\xi]^\dagger}\Big(i\partial_0 + \frac{\vec{\nabla}^2}{2M_T} - \Delta^{[\xi]}\Big)T^{[\xi]}\\ & + g^{[\xi]}\Big[T^{[\xi]^\dagger}\big(d_i\Pi_{ij}^{[\xi]}d_j\big) + h.c.\Big]\\ & + h^{[\xi]}T^{[\xi]^\dagger}\left(i\partial_0 + \frac{\vec{\nabla}^2}{2M_T}\right)^2 T^{[\xi]^\dagger} + \cdots\end{aligned} \tag{7}$$

where "…" stands for terms containing higher powers of fields and derivatives, suppressed by higher powers of the breakdown scale. The vector deuteron auxiliary field is denoted by d_i, with i index as the spin components of the deuteron. Also, the dimer auxiliary field is introduced by $T^{[\xi]}$. The m_d and $M_T = 2m_d$ are the mass of the deuteron and dimeron, respectively. We have $\eta^{[\xi]} = \pm 1$ and the $g^{[\xi]}$, $h^{[\xi]}$ and $\Delta^{[\xi]}$ are the EFT coupling constants of channel ξ. In Eq. (7), the operator $\Pi_{ij}^{[\xi]}$ is introduced as the following relations for S- and P-wave channels

$$\Pi_{ij}^{[\xi]} = \left\{\begin{array}{ll} \frac{1}{2}\delta_{ij}, & \xi = {}^1S_0\\ \frac{1}{\sqrt{6}}\varepsilon_{ij}, & \xi = {}^5S_2\\ \frac{1}{2\sqrt{2}}\varepsilon_{ijk}\mathcal{P}_k, & \xi = {}^3P_0\\ \frac{3}{2\sqrt{5}}(\delta_{ik}\delta_{jl}-\delta_{il}\delta_{jk})\varepsilon_l\mathcal{P}_k, & \xi = {}^3P_1\\ \frac{1}{\sqrt{2}}\varepsilon_{ijn}\varepsilon_{nk}\mathcal{P}_k, & \xi = {}^3P_2\end{array}\right\} \tag{8}$$

with

$$\varepsilon_i \varepsilon_j^* = \frac{1}{3}\delta_{ij} \tag{9}$$

$$\varepsilon_{ij}\varepsilon_{kl}^* = \frac{1}{10}\big(\delta_{il}\delta_{jk} + \delta_{ik}\delta_{jl} - \frac{2}{3}\delta_{ij}\delta_{lk}\big) \tag{10}$$

where σ_i with $i = 1, 2, 3$ depicts the spin Pauli matrices and $\mathcal{P}_k = \frac{1}{2i}(\overrightarrow{\nabla}_k - \overleftarrow{\nabla}_k)$.

3 Scattering amplitude

The elastic scattering amplitude of two particles in the c.m. frame interacting via short-range strong and long-range Coulomb interactions is given by

$$T(\vec{p}', \vec{p}; E) = T_C(\vec{p}', \vec{p}; E) + T_{SC}(\vec{p}', \vec{p}; E) \tag{11}$$

where T_C indicates the pure-Coulomb scattering amplitude and T_{SC} represents the scattering amplitude for the strong interaction in the pretence of the Coulomb interaction with $E = p^2/2\mu$. $\vec{p}$ and $\vec{p}'$ denote the momentum vectors of incoming and outgoing particles.

3.1 Pure-Coulomb amplitude

The pure Coulomb scattering amplitude can be written as

$$T_C(\vec{p}', \vec{p}; E) = \langle \vec{p}' | \hat{V}_C | \psi_p^{(+)} \rangle \tag{12}$$

According to the Coulomb wave function introduced in Eq. (3), the partial wave expansion of the pure Coulomb amplitude can be written as

$$\begin{aligned} T_C(\vec{p}', \vec{p}; E) &= \sum_{l=0}^{\infty} (2l+1) T_C^l(p) P_l(\hat{p}' \cdot \hat{p}) \\ &= -\frac{2\pi}{\mu} f_C(\theta) \end{aligned} \tag{13}$$

with

$$T_C^l(p) = -\frac{2\pi}{\mu}\frac{\mathrm{e}^{2i\sigma_l} - 1}{2ip} \tag{14}$$

where $\cos\theta = \hat{p}\cdot\hat{p}'$ and $p = |\vec{p}| = |\vec{p}'|$. The explicit solution leads to the well-known Mott scattering cross section

$$f_C(\theta) = -\frac{\eta_p^2}{2k_C}\csc^2(\theta/2)\exp\Big[2i\sigma_0 - 2i\eta_p \ln(\sin(\theta/2))\Big] \tag{15}$$

which holds at very low energies.

3.2 Coulomb-subtracted scattering amplitude

The strong scattering amplitude modified by Coulomb corrections is

$$T_{SC}(\vec{p}', \vec{p}; E) = \langle \psi_{p'}^{(-)} | \hat{V}_S | \Psi_p^{(+)} \rangle \tag{16}$$

where $\hat{V}_S$ is strong interaction operator and $\Psi_p^{(\pm)}$ denotes the incoming/outgoing state of Coulomb-distorted interaction. T_{SC} amplitude can be expressed in the partial wave decomposition

$$\begin{aligned} T_{SC}(\vec{p}', \vec{p}; E) &= \sum_{l=0}^{\infty} (2l+1) T_{SC}^l(p)\, \mathrm{e}^{2i\sigma_l} P_l(\hat{p}' \cdot \hat{p}) \\ &= -\frac{2\pi}{\mu} f_{SC}(\theta) \end{aligned} \tag{17}$$

with

$$T_{SC}^l(p) = -\frac{2\pi}{\mu}\frac{e^{2i\delta_l} - 1}{2ip} = -\frac{2\pi}{\mu}\frac{1}{p\cot\delta_l - ip} \tag{18}$$

in terms of the Coulomb-corrected phase shift δ_l. The Coulomb-subtracted phase shift δ_l is usually expressed in terms of a modified effective range expansion (ERE) as (Goldberger and Watson, 2004)

$$\begin{aligned} T_{CS}^{[l]}(p) = &-\frac{2\pi}{\mu}\times \\ &\frac{C_0^2(\eta_p)\, W_l(\eta_p)}{-\frac{1}{a_l} + \frac{1}{2}r_l\, p^2 + \frac{1}{4}s_l\, p^4 + \cdots - 2k_C W_l(\eta_p) H(\eta_p)} \end{aligned} \tag{19}$$

where a_l, r_l, and s_l are the scattering length, effective range, and shape parameter and we have

$$W_l(\eta_p) = \frac{k_C^{2l}}{(l!)^2}\prod_{n=0}^{l}(1 + \frac{n^2}{\eta_p^2}) \tag{20}$$

$$H(\eta_p) = \psi(i\eta_p) + \frac{1}{2i\eta_p} - \ln(i\eta_p) \tag{21}$$

where the function ψ is the logarithmic derivative of Γ-function.

3.3 EFT scattering amplitudes up to NLO

The building block of the d-d scattering amplitude is the full propagator of the dimeron as shown in Fig. 2. The EFT diagram of the d-d elastic scattering amplitude without contributions of $p-t$ and $n-\tau$ interactions up to NLO is shown in Fig. 2. The bare and full propagators of $T^{[\xi]}$ are depicted by the thick dashed line and the thick dashed line with filled circle, respectively.

According to the suggested PC in Table 1, the LO contribution of Coulomb-subtracted d-d scattering for channel ξ can be obtained by considering first three terms in Lagrangian (Eq. (7)) and the last term initially enters as NLO corrections. In order to evaluate the cluster EFT results for the d-d elastic scattering amplitude in channel ξ, the external legs should be attached to the full dimeron propagator as shown in the first line of Fig. 2. So, the S- and P-wave Coulomb-subtracted EFT amplitudes up to N^{n}LO ($n = 0, 1$) can be determined by

$$-iT_{SC}^{[n,\xi]}(p)\, e^{2i\sigma_0} = -i\, g^{[\xi]^2}\mathcal{D}^{[n,\xi]}(E, \vec{0})\, C_0^2(\eta_p)\, \mathrm{e}^{2i\sigma_0} \tag{22}$$

for $\xi = {}^1S_0$, ${}^5S_2$ channels and

$$\begin{aligned} &-i\,3\,T_{SC}^{[n,\xi]}(p)\mathrm{e}^{2i\sigma_1}\hat{p}\cdot\hat{p}' \\ &= -i\, g^{[\xi]^2}\mathcal{D}^{[n,\xi]}(E, \vec{0})\, C_0^2(\eta_p)(p^2 + k_C^2)\, \mathrm{e}^{2i\sigma_1}\hat{p}\cdot\hat{p}' \end{aligned} \tag{23}$$

for ${}^3P$ channel. We emphasize that the relations Eq. (22) and Eq. (23) are derived using expressions in Eq. (4). According to Fig. 2, the N^{n}LO ($n = 0, 1$) full dimeron

propagator for channel ξ in c.m. frame can be evaluated by

$$\mathcal{D}^{[n,\xi]}(E,\vec{0}) = \frac{\eta^{[\xi]}}{E-\Delta^{[\xi]}-\eta^{[\xi]}\Sigma^{[\xi]}(E)} \times \left(1 - n\frac{\eta^{[\xi]} g_2^{[\xi]} E^2}{E-\Delta^{[\xi]}-\eta^{[\xi]}\Sigma^{[\xi]}(E)}\right) \tag{24}$$

with

$$\Sigma^{[\xi]}(E) = \frac{1}{2l+1} g^{[\xi]^2} J_l(E). \tag{25}$$

The J_l function is divergent and should be regularized. We regularize the divergence by dividing the J_l function into two finite and infinite parts as $J_l = J_l^{fin} + J_l^{div}$. The finite terms of the functions J_0 and J_1 for S- and P-wave states are obtained as (Kong and Ravndal, 1999; Higa et al., 2008)

$$J_0^{fin}(p) = -\frac{k_C \mu}{\pi} H(\eta_p), \tag{26}$$

$$J_1^{fin}(p) = -\frac{k_C \mu}{\pi}(p^2 + k_C^2) H(\eta_p). \tag{27}$$

The divegent part is momentum independent for S waves and for the P wave are sum up momentum independent and momentum squared parts. These divergences absorbed in $\Delta^{[\xi]}$, $g^{[\xi]}$ and $h^{[\xi]}$ parameters via introducing the renormalized parameters $\Delta_R^{[\xi]}$, $g_R^{[\xi]}$ and $h_R^{[\xi]}$. Consequently, the EFT scattering amplitude for the S channels ($^3S_1$, $^5S_2$) and ^3P channels up to NLO can be written as

$$T_{SC}^{[n,\xi]}(p) = -\frac{2\pi}{\mu} \frac{C_0^2(\eta_p)}{\frac{2\pi\Delta_R^{[\xi]}}{\eta^{[\xi]} g^{[\xi]^2}\mu} - \frac{1}{2}\left(\frac{2\pi}{\eta^{[\xi]} g^{[\xi]^2}\mu^2}\right) p^2 - 2k_C H(\eta_p)} \times \underbrace{\left[1}_{\text{LO}} + \underbrace{\frac{1}{4} n \frac{\left(\frac{2\pi h^{[\xi]}}{g^{[\xi]^2}\mu^3}\right)}{\frac{2\pi\Delta_R^{[\xi]}}{\eta^{[\xi]} g^{[\xi]^2}\mu} - \frac{1}{2}\left(\frac{2\pi}{\eta^{[\xi]} g^{[\xi]^2}\mu^2}\right) p^2 - 2k_C H(\eta_p)} p^4}_{\text{NLO corection}}\right] \tag{28}$$

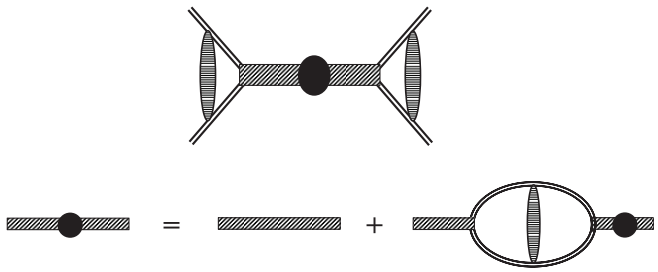

Figure 2: The amplitude of the two-deuteron elastic scattering. The thick dashed line is the bare dimeron propagator and the thick dashed line with a filled circle represents the full dimeron propagator. All remained notations are as in Fig. 1.

and

$$T_{SC}^{[n,\xi]}(p) = -\frac{2\pi}{\mu} \frac{C_0^2(\eta_p)(p^2+k_C^2)}{\frac{6\pi\Delta_R^{[\xi]}}{\eta^{[\xi]} g_R^{[\xi]^2}\mu} - \frac{1}{2}\left(\frac{6\pi}{\eta^{[\xi]} g_R^{[\xi]^2}\mu^2}\right) p^2 - 2k_C(p^2+k_C^2) H(\eta_p)} \times \underbrace{\left[1}_{\text{LO}} + \underbrace{\frac{1}{4} n \frac{\left(\frac{6\pi h_R^{[\xi]}}{g_R^{[\xi]^2}\mu^3}\right)}{\frac{6\pi\Delta_R^{[\xi]}}{\eta^{[\xi]} g_R^{[\xi]^2}\mu} - \frac{1}{2}\left(\frac{6\pi}{\eta^{[\xi]} g_R^{[\xi]^2}\mu^2}\right) p^2 - 2k_C(p^2+k_C^2) H(\eta_p)} p^4}_{\text{NLO corection}}\right] \tag{29}$$

respectively. Comparing Eqs. (28) and (29) with ERE expansion of Eq. (19) yields

$$\Delta_R^{[\xi]} = -\frac{\mu\eta^{[\xi]} g^{[\xi]^2}}{2\pi a^{[\xi]}}, \quad g^{[\xi]^2} = -\frac{2\pi}{\mu^2 \eta^{[\xi]} r^{[\xi]}}, \quad h^{[\xi]} = -\frac{\mu^3 g^{[\xi]^2} s^{[\xi]}}{2\pi} \tag{30}$$

for $^3S_1$ and $^5S_2$ channels and

$$\Delta_R^{[\xi]} = -\frac{\mu\eta^{[\xi]} g_R^{[\xi]^2}}{6\pi a^{[\xi]}}, \quad g_R^{[\xi]^2} = -\frac{6\pi}{\mu^2 \eta^{[\xi]} r^{[\xi]}}, \quad h_R^{[\xi]} = -\frac{\mu^3 g_R^{[\xi]^2} s^{[\xi]}}{6\pi} \tag{31}$$

for ^3P channels. The unknown bare and renormalized EFT LECs in Eqs. (30) and (31) and also sign of the parameter $\eta^{[\xi]}$ should be initially determined by matching EFT expression of phase shift and cross section to the available experimental data.

4 EFT coupling constants determination

As previously explained, in the low-energy region for the d-d scattering the S- and P-wave channels ($\xi = {}^1S_0$, $^5S_2$, ^3P) dominantly contribute in the total scattering cross section. Calculating the physical scattering observables e.g., phase shifts and cross section, based on the cluster EFT expressions needs to determine the values of the LECs in Lagrangian (Eq. (7)). Determination of the EFT LECs for the S and P partial waves are presented in the following subsections.

Table 2: The determined S-wave effective range parameters. The parameters obtain from fits to the low-energy phase shifts data in Ref. (Meier and Glöckle, 1975). The shape parameters $s^{[\xi]}$ is only used at the NLO fits. $\chi^{[\xi]^2}$ is as described in the text.

ξ	order	$a^{[\xi]}$ [fm]	$r^{[\xi]}$ [fm]	$s^{[\xi]}$ [fm^3]	$\chi^{[\xi]^2}$
$^1S_0$	LO	4.3825	0.8135	0	0.0023
	NLO	4.3170	3.0702	340.021	0.0026
$^5S_2$	LO	6.1436	1.6234	0	0.0066
	NLO	6.1428	1.6372	2.1513	0.0066

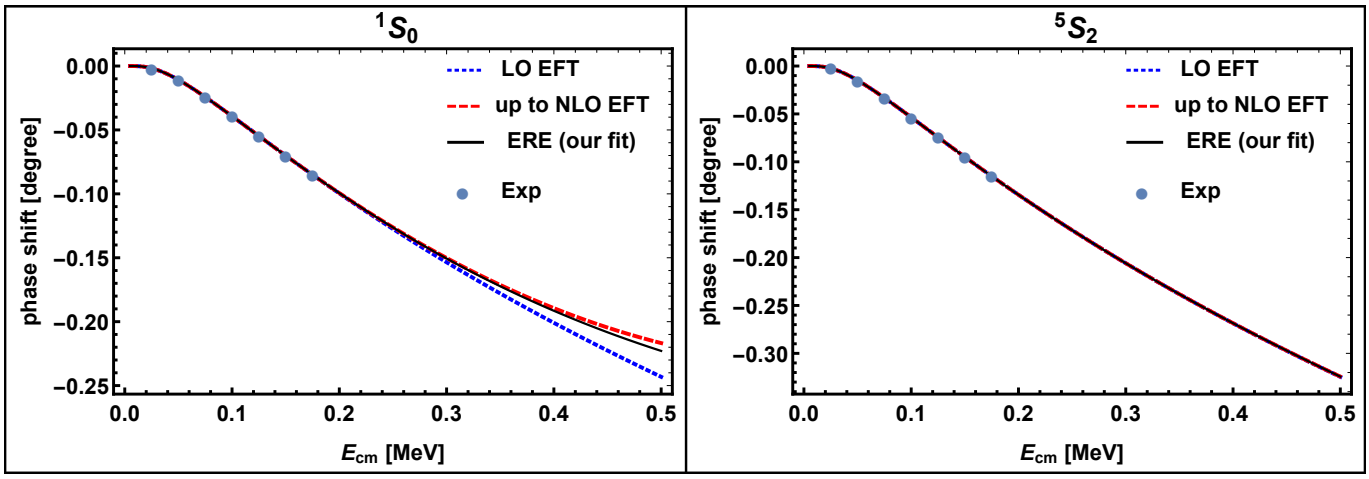

Figure 3: (color online) Comparison of the ERE fits and halo EFT calculations for the $^1S_0$ and $^5S_2$ d-d elastic scattering phase shifts with the results from Ref. (Meier and Glöckle, 1975). Dots is the results in (Meier and Glöckle, 1975) and the solid, dotted and dashed lines denote the calculations of ERE, LO EFT and NLO EFT, respectively.

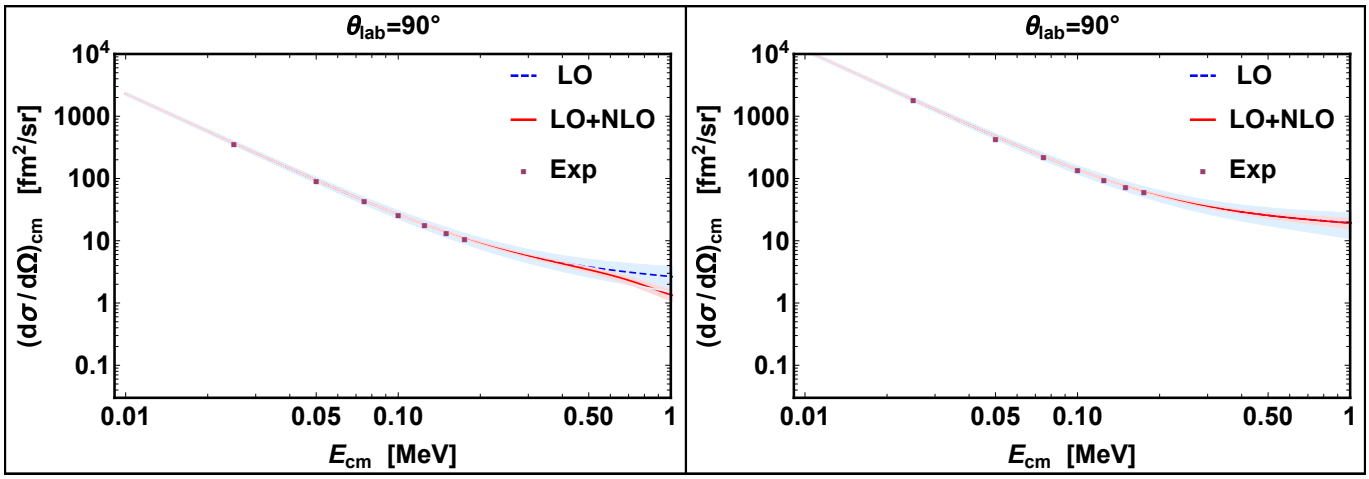

Figure 4: (color online) The fit of the halo EFT calculations for the ^3P d-d elastic differential cross section to the results from Ref. (ENDF/B, 2022). Dots is the results in Ref. (ENDF/B, 2022). The solid, dotted and dashed lines denote the calculations of ERE, LO EFT and NLO EFT, respectively. The light blue and red bands denote the systematical EFT uncertainties of the LO and LO+NLO EFT results.

4.1 $l = 0$ partial waves

This constructed cluster EFT for two deuterons system is reliable at the incident c.m. energies below 2 MeV. For the energy range of order few ten keV, a phase shift analysis was reported for d-d elastic scattering in the $l = 0$ channels with spin 0 and 2 in Ref. Meier and Glöckle (1975). This existing phase shift data for $\xi = {}^1S_0$, $^5S_2$ channels at very low energies help us to obtain the values of LECs of the S-waves. Using Eq. (18), the Coulomb-modified phase shift in terms of the on-shell scattering amplitude for channel ξ up to N^{n}LO ($n = 0, 1$) is given by

$$\delta^{[\xi]}(p) = \cot^{-1}\Big(-\frac{2\pi}{\mu p}\mathrm{Re}\big([T_{CS}^{[n,\xi]}(p)]^{-1}\big)\Big). \tag{32}$$

Fitting the relations Eq. (32) to the available phase shift data for two S partial waves of Ref. (Meier and Glöckle, 1975), we obtain the values of the effective range parameters at LO and up to NLO. The effective range parameters of $^1S_0$ and $^5S_2$ channels have been obtained depending on our explained fits as reported in Table 2. As seen from Table 2, in each channel, we use the power counting that the scattering amplitudes gets LO contributions from scattering length and effective range and correction of the shape parameter enters at NLO. The quality of description of available results F^{ava} on the basis of the certain expression F can be estimated by the χ^2 method which is written as

$$\chi^2 = \frac{1}{N}\sum_{i=1}^{N}\left[\frac{F_i - F_i^{ava}}{F_i^{ava}}\right]^2 \tag{33}$$

where N is the number of measurements. Taking into consideration F as $\delta^{[\xi]}$ introduced in Eq. (32), the deviations of fits from used phase shift results for ξ channel are obtained as shown in the last column of Table 2 by $\chi^{[\xi]^2}$. Now, using the obtained LO and NLO values of effective range parameters presented in Table 2, the LO and up to

Table 3: The EFT LECs for all channels. The LO ($n = 0$) and NLO ($n = 1$) values of the EFT coupling constants determined by using the obtained values of the effective range parameters presented in Table 2. The third row in each channel indicates our suggested power-counting estimations for evaluated EFT LECs with $Q \sim k_C$ and $\Lambda \sim 90$ MeV.

ξ	n	$g^{[\xi]}$ [MeV$^{-l-1/2}$]	$\Delta_R^{[\xi]}$ [MeV]	$h^{[\xi]}$ [MeV^{-1}]	$\eta^{[\xi]}$
$^1S_0$	0	0.0415	11.6071	0	-1
	1	0.0214	3.1221	2.6761	-1
	PC estimation	0.0179	4.3186	2.9771	–
$^5S_2$	0	0.0294	4.1490	0	-1
	1	0.0293	4.1145	0.0317	-1
	PC estimation	0.0179	4.3186	0.2316	–
ξ	n	$g_R^{[\xi]}$ [MeV$^{-l-1/2}$]	$\Delta_R^{[\xi]}$ [MeV]	$h_R^{[\xi]}$ [MeV^{-1}]	$\eta^{[\xi]}$
^3P	0	0.0287	1.6251	0	$+1$
	1	0.0248	1.2384	8705.97	$+1$
	PC estimation	0.0329	4.3186	6327.51	–

NLO values of EFT LECs for spin 0 and 2 channels are determined as indicated in the first and second rows of Table 3. The estimation of our used power-counting for the LECs of each channel presented as "PC estimation" in Table 3. The orders of obtained EFT LECs are meaningfully consistent with the predictions of suggested PC. The obtained EFT phase shifts of two deuterons scattering in S-wave channels are shown in Fig. 3. The LO (up-to-NLO) EFT and fitted ERE results of two S-wave phase shifts are plotted against c.m. energy by dotted (dashed) and solid lines, respectively. In Fig. 3, the circles indicate the phase shift data from Ref. (Meier and Glöckle, 1975). We considered the d-d elastic scattering pase shifts in the energy range below 1 MeV in the c.m. frame, which are sufficient for solving various problems, in particular, evaluating the differential cross sections at the valid EFT range.

4.2 $l = 1$ partial waves

Lack of the phase shift analysis and experimental data for $l = 1$ channel at low energies causes to use the available cross section data to find the values of the ^3P coupling constants. The differential scattering cross section of two deuterons is given by (ENDF/B, 2022)

$$\frac{d\sigma(\theta)}{d\Omega} = \frac{1}{9}\sum_S (2S+1)\Big|f(\theta) + (-1)^S f(\pi-\theta)\Big|^2 \qquad (34)$$

where $f(\theta) = f_C(\theta) + f_{SC}(\theta)$. The scattering amplitudes f_C and f_{SC} are described in Sec. 3. Inserting the EFT amplitudes Eqs. (22) and (23) for S and P waves into Eq. (17), and using the obtained values of EFT LECs for $^1S_0$ and $^5S_2$ channels, we can match the EFT expression for the differential cross section of d-d elastic scattering to the reported experimental data in Ref. (ENDF/B, 2022) for the c.m. scattering angle $\theta_{cm} = 90^\circ$ and find the ^3P coupling constants. The fits lead to the determined values presented in the last row of Table 3. The LO and up-to-NLO EFT fits to differential cross section data in Ref. (ENDF/B, 2022) are shown in Fig. 4.

Based on described power-counting, we consider the coupling constants corresponding to the scattering length and effective range at LO calculation and the shape parameter effect enters at NLO by inserting the last term of Lagrangian (Eq. (7)) containing the $h^{[\xi]}$ coupling constant. Our PC estimations for the order of values of the EFT LECs are also shown in Table 3. Determined values have good consistency with used PC as presented in Table 3.

5 Results

Taking into account the determined values of EFT LECs presented in Table 3, we can compute the differential cross section at different incident energies and scattering angles. We recall that we use the pure d-d channel in which the influence of other p-t and n-τ interactions is not taken into consideration.

In order to calculate the differential cross section for the low-energy d-d elastic scattering, some important issues should be clarified. At low energies the cross section gets dominant contributions from S and P waves scattering. According to phase shift analysis and available phase shift results, the leading term in the d-d scattering cross section is from S-wave spin quintet channel $^5S_2$. However, both S-wave spin singlet and P-wave spin triplet channels enter first at NLO as presented by our suggested PC in Table 1. Contribution of each spin channel in the cross section shown in Fig. 5.

On the other hands, regarding to the phase shift analysis for all S- and P-wave channels, the leading d-d scattering cross section constructed by the corresponding relation to the scattering length of $^5S_2$ channel. The NLO corrections of the d-d scattering cross section get the contributions from the scattering length and the effective range of $^1S_0$ and the effective range of $^5S_2$ partial wave. Remained partial-wave parameters first enter at N^{2}LO and higher orders.

Our results for the differential cross sections of the d-d elastic scattering against c.m. energy with laboratory

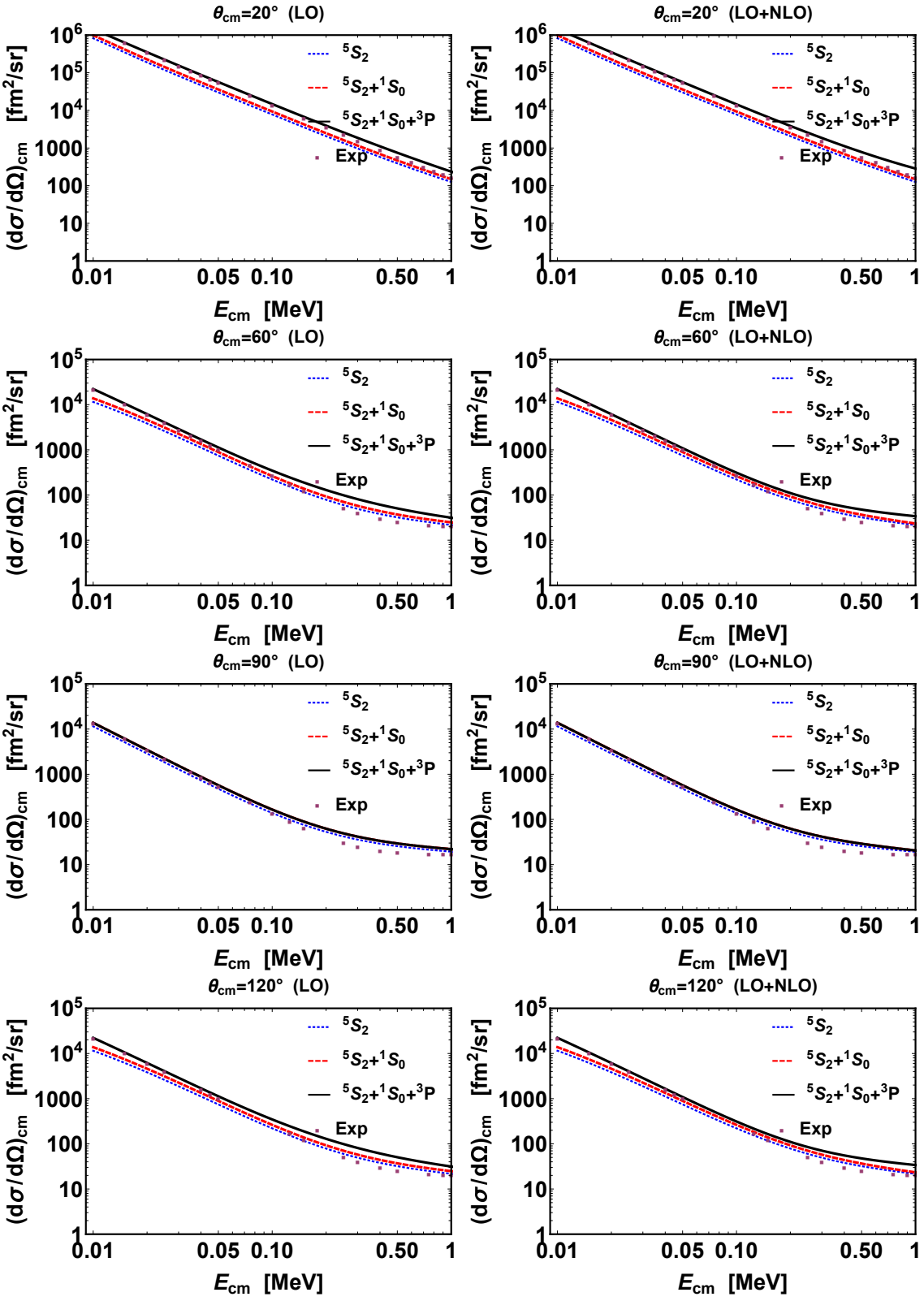

Figure 5: (color online) The differential cross section of elastic scattering of d-d vs c.m. energy E_{cm}. The graphs have been plotted with the outgoing deuteron angles in laboratory system $\theta_{lab} = 20^\circ$, $\theta_{lab} = 60^\circ$, $\theta_{lab} = 90^\circ$ and $\theta_{lab} = 120^\circ$ respectively. Symbols are the experimental data of (ENDF/B, 2022). The red dotted, blue dashed and black solid lines are the d-d scattering cross section with $S = 2$, $S = 0$, 2 and $S = 0$, 1, 2 channels, respectively. The left (right) plots are concluded from only LO (LO+NLO) terms of each spin channels, respectively.

scattering angles $\theta_{lab} = 20^\circ$, 60°, 90° and 120° are shown in Fig. 5. The LO and NLO EFT results are depicted by the dashed and solid lines, respectively. We have also plotted the differential cross section versus the c.m. scattering angle for the d-d scattering in Fig. 6 for incident deuteron energy $E_d = 50$ and 100 keV. The dashed and solid lines

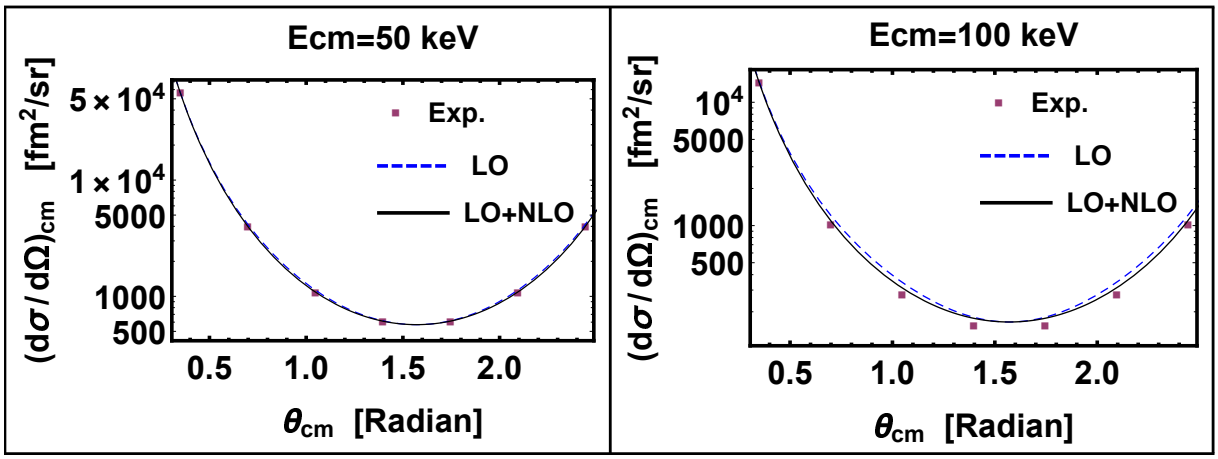

Figure 6: (color online) The differential cross section of elastic scattering of d-d vs c.m. energy θ_{cm} with incident deuteron energies $E_d = 50$ and 100 keV. Symbols are the experimental data of (ENDF/B, 2022). The blue dashed and black solid lines are the the LO and LO+NLO EFT results as explained in the text.

represent our LO and NLO EFT results, respectively.

6 Conclusion and outlook

In this paper, we have studied the low-energy two deuterons scattering using cluster EFT. Our constructed cluster EFT treats the deuterons as the point-like nuclear clusters, so we concentrated on the energy region $0 < E_{cm} < 1$ MeV. At the present energy region, the Coulomb force have been considered as a non-perturbative treatment.

We have shown that a PC can be formulated that leads to consistent renormalization. Based on our suggested PC, the LO contributions of phase shift in each partial wave have been constructed from its scattering length and effective range and its shape parameter influences have been included at the NLO. Using the available phase shift results for both S waves, we obtained the values of the effective range parameters for these states. The EFT LECs for $l = 0$ partial waves evaluated in terms of effective range parameters. With respect to no existing the phase shift data for the ^3P channels, we used the differential cross section data at a fixed scattering angle to determine the EFT coupling constants for these chanels. We note that the effects of the p-t and n-τ interactions are negligible up to NLO and have not been included in the present calculation. Our ERE fitted curves and the cluster EFT calculations for the S-wave phase shifts and elastic differential cross section have good consistency with the available results, and a converging pattern from LO to NLO.

Considering our used PC, the cross sections of the d-d scattering got the LO contributions from the $^5S_2$ channel and other $^1S_0$ and ^3P channels enter at NLO. We have plotted the LO and NLO differential cross sections against the c.m. scattering angle and also the incident total energy. The comparison to the experimental data indicates good consistency of our EFT evaluations.

It would be interesting to use our results for the d+d $\rightarrow^4$He+γ astrophysical radiative capture based on cluster EFT calculation. The effects of including the the $p-t$ and $n-\tau$ interactions could be considered to study the d+d$\rightleftharpoons$ p+τ and d+d$\rightleftharpoons$ n+t processes in the future. The d-d scattering and radiative capture can also be studied by the three- four-body EFT formalism.

Conflict of Interest

The authors declare no potential conflict of interest regarding the publication of this work.

References

Ando, S.-I. (2014). The Born series for S-wave quartet nd scattering at small cutoff values. *Few-Body Systems*, 55(3):191–201.

Ando, S.-I. (2016). Elastic C-12 scattering at low energies in cluster effective field theory. *The European Physical Journal A*, 52(5):1–8.

Ando, S.-I. and Birse, M. C. (2008). Renormalization-group analysis for low-energy scattering of charged particles. *Physical Review C*, 78(2):024004.

Ando, S.-i., Shin, J. W., Hyun, C. H., et al. (2007). Low energy proton-proton scattering in effective field theory. *Physical Review C*, 76(6):064001.

Ando, S.-I., Yang, G.-S., and Oh, Y. (2014). λ-λ H-4 in halo effective field theory. *Physical Review C*, 89(1):014318.

Arani, M. M. (2020). Low-energy scattering of deuteron by He-3 3 He and H-3 3 H in halo effective field theory. *The European Physical Journal A*, 56(8):1–11.

Arani, M. M., Koohi, A., and Yarmahmoodi, S. (2017a). $d + t \rightarrow n + \alpha$ fusion reaction in a model inspired by halo/cluster effective field theory. *International Journal of Modern Physics E*, 26(12):1750080.

Arani, M. M., Radin, M., and Bayegan, S. (2017b). n+ n+ $\alpha \rightarrow^6 He+\gamma$ reaction by effective field theory approach. *Progress of Theoretical and Experimental Physics*, 2017(9):093D07.

Barford, T. and Birse, M. C. (2003). Renormalization group approach to two-body scattering in the presence of long-range forces. *Physical Review C*, 67(6):064006.

Bedaque, P., Hammer, H.-W., and Van Kolck, U. (2003). Narrow resonances in effective field theory. *Physics Letters B*, 569(3-4):159–167.

Bedaque, P. F. and Van Kolck, U. (2002). Effective field theory for few-nucleon systems. *Annual Review of Nuclear and Particle Science*, 52(1):339–396.

Bertulani, C., Hammer, H.-W., and Van Kolck, U. (2002). Effective field theory for halo nuclei: shallow p-wave states. *Nuclear Physics A*, 712(1-2):37–58.

Braaten, E. and Hammer, H.-W. (2006). Universality in few-body systems with large scattering length. *Physics Reports*, 428(5-6):259–390.

Burke, P. and Laskar, W. (1961). Four Nucleon Reactions with Central Forces. *Proceedings of the Physical Society (1958-1967)*, 77(1):49.

Chen, J.-W., Rupak, G., and Savage, M. J. (1999). Nucleon-nucleon effective field theory without pions. *Nuclear Physics A*, 653(4):386–412.

Chwieroth, F., Tang, Y., and Thompson, D. (1972). Study of d+d scattering with the resonating-group method and an imaginary potential. *Nuclear Physics A*, 189(1):1–19.

ENDF/B (2022). *ENDF/B online database at the NNDC Online Data Service, http://www.nndc.bnl.gov*. Evaluated Nuclear Data File (ENDF).

Gasser, J., Lyubovitskij, V. E., and Rusetsky, A. (2008). Hadronic atoms in QCD+ QED. *Physics Reports*, 456(5-6):167–251.

Goldberger, M. L. and Watson, K. M. (2004). *Collision theory*. Courier Corporation.

Hammer, H., Ji, C., and Phillips, D. (2017). Effective field theory description of halo nuclei. *Journal of Physics G: Nuclear and Particle Physics*, 44(10):103002.

Higa, R., Hammer, H.-W., and van Kolck, U. (2008). $\alpha - \alpha$ scattering in halo effective field theory. *Nuclear Physics A*, 809(3-4):171–188.

Higa, R., Rupak, G., and Vaghani, A. (2018). Radiative He-3$(\alpha, \gamma\alpha, \gamma)$Be-7 reaction in halo effective field theory. *The European Physical Journal A*, 54(5):1–12.

Ji, C., Elster, C., and Phillips, D. (2014). He-6 nucleus in halo effective field theory. *Physical Review C*, 90(4):044004.

Kaplan, D. B., Savage, M. J., and Wise, M. B. (1998). Two-nucleon systems from effective field theory. *Nuclear Physics B*, 534(1-2):329–355.

Kong, X. and Ravndal, F. (1999). Proton–proton scattering lengths from effective field theory. *Physics Letters B*, 450(4):320–324.

Kong, X. and Ravndal, F. (2000). Coulomb effects in low energy proton–proton scattering. *Nuclear Physics A*, 665(1-2):137–163.

Lensky, V. and Birse, M. C. (2011). Coupled-channel effective field theory and proton-^{7}Li scattering. *The European Physical Journal A*, 47(11):1–10.

Marlinghaus, E., Genz, H., Pospiech, G., et al. (1975). Elastic scattering 2H(d, d)2H below 360 keV:(I). Experiment. *Nuclear Physics A*, 255(1):13–20.

Meier, W. and Glöckle, W. (1975). Elastic scattering ^{2}H(d, d)^{2}H below 360 keV:(II). Theory. *Nuclear Physics A*, 255(1):21–34.

Niewisch, J. and Fick, D. (1975). Elastic deuteron-deuteron scattering at low bombarding energies. *Nuclear Physics A*, 252(1):109–119.

Phillips, D. R., Rupak, G., and Savage, M. J. (2000). Improving the convergence of NN effective field theory. *Physics Letters B*, 473(3-4):209–218.

Thompson, D. (1970). Study of the d+d system using the method of resonating-group structure. *Nuclear Physics A*, 143(2):304–314.

Weiss, G. H. (1958). Quantum Mechanics. Non-relativistic theory. LD Landau and EM Lifshitz. vol. 3, of Course of Theoretical Physics. Translated by JB Sykes and JS Bell. Pergamon Press, London; Addison Wesley, Reading, Mass., 1958. xii+ 515 pp. 12.50. *Science*, 128(3327) : 767 − −768.

Xuan, Z. and Fan-An, Z. (1985). Soft repulsive core effects in (d+d) scattering and reaction. *Nuclear science and Engineering*, 89(4):351–361.

To cite this article:

Farzin, M., Radin, M., Moeini Arani, M. (2023). Low-energy deuteron-deuteron elastic scattering in cluster effective field theory. *Radiation Physics and Engineering*, 4(1), 29-38

DOI: 10.22034/rpe.2022.371177.1109

To link to this article: https://doi.org/10.22034/rpe.2022.371177.1109